Thermal conductivity of one-dimensional carbon-boron nitride van der Waals heterostructure: A molecular dynamics study

Han Meng [a,b], Shigeo Maruyama [b], Rong Xiang [b,*], Nuo Yang [a,*]

[a] State Key Laboratory of Coal Combustion, School of Energy and Power Engineering, Huazhong University of Science and Technology, Wuhan 430074, China.
[b] Department of Mechanical Engineering, The University of Tokyo, 7-3-1 Hongo, Bunkyo-ku, Tokyo 113-8656, Japan.

ARTICLE INFO

ABSTRACT

Investigating thermal transport in van der Waals heterostructures is of scientific interest and practical importance for their applications in a broad range. In this work, thermal conductivity of one-dimensional heterostructure consisting of carbon and boron nitride nanotubes is systematically investigated via molecular dynamics simulations. Thermal conductivity is found to have strong dependences on temperature, length and diameter. In addition, the axial strain and intensity of van der Waals interaction are demonstrated to be able to modulate thermal conductivity up to about 43% and 37%, respectively. Moreover, the dependence of thermal conductivity on the chirality of constituent nanotubes is studied. These results are explained based on lattice dynamics insights. This work not only provides feasible strategies to modulate thermal conductivity, but also enhances the understanding of the fundamental physics of phonon transport in one-dimensional heterostructures.

1. Introduction

The van der Waals (vdW) heterostructure with different atomic layers stacked beyond symmetry and lattice matching through vdW interaction, has been considered as a promising candidate in a wide application range such as electronics, thermoelectrics and optics [1–3]. To the current state of art, dimensionality of heterostructure is decreased but mainly limited to two-dimensional (2D) form composed of different planar layers like graphene, monolayer boron nitride, phosphorene and transition metal dichalcogenides [4]. Most recently, the limitation of dimension has been experimentally broken, generating a new class of heterogeneous material named one-dimensional (1D) vdW heterostructure [5]. By combining the advantages of different nanotubes such as carbon nanotube (CNT), boron nitride nanotube (BNNT) and chalcogenide nanotube, it is hopeful to arouse new properties and broaden the application of 1D heterostructures [6–9].

Investigating thermal transport in heterostructures is of scientific interest and practical importance for applications like heat dissipation, thermoelectric materials and electronics packaging [10–12]. Tremendous efforts have been devoted to the research on thermal transport in 2D heterostructures over the past years. Liu et al. designed a phosphorene-graphene heterostructure and achieved high interfacial thermal conductance that can be tuned by tensile strain [10]. Ren et al. demonstrated that interfacial thermal resistance is significantly reduced in phononic-mismatched heterostructures and interfacial thermal conductance has a weak temperature dependence, which is different from that of conventional heterostructures achieved by interfacing dissimilar materials [11]. Cai et al. found that BN dominates the thermal transport in BN-silicene bilayer heterostructure due to the weak interaction between two layers [12]. However, study on the thermal transport in 1D heterostructure is lacking and the thermal properties and physical mechanisms remains to be discovered [13]. Noting that thermal transport can behave abnormally with the decrease of dimension, to be specifically, phonons propagate ballistically in 1D structures rather than diffusively in 2D systems and beyond [14]. Given that, thermal transport in 1D heterostructures is supposed to be different from that in 2D systems. Therefore, there is a great importance and necessity to study thermal conductivity of 1D heterostructures.

In this work, thermal conductivity of 1D heterostructure consisting of CNT and BNNT (denoted as CNT@BNNT) is numerically studied by non-equilibrium molecular dynamics simulations. Firstly, CNT@BNNT with different sizes and different chiral constituent nanotubes are constructed. Subsequently, temperature, length and diameter dependence of thermal conductivity are studied. Then, axial strain and intensity of vdW interaction are intro-
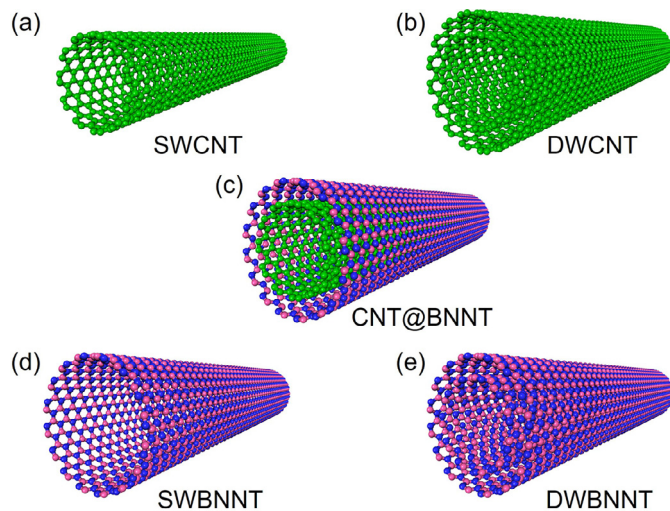
Fig. 1. Atomic structure of (a) single-wall CNT, (b) double-wall CNT, (c) 1D vdW heterostructure CNT@BNNT, (d) single-wall BNNT and (e) double-wall BNNT. The pink, blue and green spheres represent boron, nitrogen and carbon atoms, respectively.

duced to modulate thermal conductivity. Lattice dynamics analysis is carried out to explain the strain effect and the influence of the intensity of vdW interaction on thermal conductivity by quantifying phonon density of states. Lastly, the influence of chirality of constituent CNT and BNNT on thermal conductivity is studied and the outlook of future research is proposed.

2. Model and method

Similar to the double-wall CNT (DWCNT) and double-wall BNNT (DWBNNT), the one-dimensional CNT@BNNT heterostructure (as shown in **Fig. 1c**) is constructed by coaxially nesting a single-wall CNT (SWCNT) into a single-wall BNNT (SWBNNT). The inter-wall distance of 3.4 Å between inner SWCNT and outer SWBNNT, equaling to the equilibrium interlayer distance of graphene and monolayer boron nitride results from vdW interaction, is generated by the construction procedure. In the following calculation, CNT@BNNT heterostructure consisting of (11, 11) CNT and (16, 16) BNNT is chosen as the smallest structure, where the length and the inner diameter (diameter of inner CNT) are 10 nm and 1.5 nm, respectively. Noting that CNT@BNNT heterostructure is one-dimensional, we only focus on the thermal conductivity along axial direction.

The classical non-equilibrium molecular dynamics (NEMD) method has been employed in the calculation of thermal conductivity [15–20]. The heat source with higher temperature and heat sink with lower temperature are applied to left and right region next to the fixed ends, respectively (as illustrated in **Fig. S1**). After obtaining the steady temperature profile and heat current, thermal conductivity can be calculated based on the Fourier's law of heat conduction as

$$\kappa = -\frac{J}{A\nabla T}, \tag{1}$$

where A is the cross-sectional area defined as the ring with a thickness of 6.8 Å, which equals to the double equilibrium interlayer distance resulting from van der Waals interaction between inner and outer wall. ∇T is the time-averaged temperature gradient along axial direction. J is the heat flux that recorded by the average of the input and output power of the two baths as

$$J = \frac{\Delta E_{bath} + \Delta E_{sink}}{2\Delta t}, \tag{2}$$

where ΔE is the energy flow from heat bath or flow into heat sink during each time step Δt.

All simulations are performed by the large-scale atomic/molecular massively parallel simulator (LAMMPS) package [21–25]. The interatomic interaction within nanotubes is described by Tersoff potential, which includes both two-body and three-body terms and has been widely used to study the thermal properties [26,27]. The Lennard-Jones (LJ) potential is implemented for the van der Waals interaction between BNNT and CNT. The LJ parameters are extracted from the Universal Force Field, parameters across different types of atoms are calculated by using the Lorentz-Berthlot mixing rules [28]. Two Langevin thermostats with a temperature difference of 20 K are used to establish temperature gradient along axial direction. The fixed and periodic boundary conditions are applied in axial and other two directions, respectively. Time step is set as 0.5 fs, and the velocity Verlet algorithm is used to integrate the discrete differential equations of motion [29]. To overcome the statistical error, the results are averaged over five independent simulations with different initial conditions. (More simulation details are given in **supplementary material**)

3. Results and discussion

Firstly, thermal conductivity of CNT@BNNT is calculated at the temperature of 300 K, where the length and the inner diameter are 10 nm and 1.5 nm, respectively. As a result, room-temperature thermal conductivity is obtained as high as 371.61±7.03 Wm^{-1}K^{-1}. The value is at the same order of magnitude as other nanotubes such as CNT and BNNT. For a better comparison, thermal conductivity of SWBNNT and SWCNT extracted from CNT@BNNT, DWBNNT and DWCNT and BNNT@CNT with the same size as CNT@BNNT are calculated, the results are shown in **Fig. 2a**. Thermal conductivity of CNT@BNNT is higher than the value of SWBNNT (277.83±5.67 Wm^{-1}K^{-1}) but lower than that of SWCNT (553.84±14.14 Wm^{-1}K^{-1}). It is reasonable to obtain an intermediate thermal conductivity value when combining two different materials, which reflect the compromise of thermal conductivity of two different materials. Similarly, thermal conductivity of CNT@BNNT also falls in between the values of DWBNNT (271.48±11.28 Wm^{-1}K^{-1}) and DWCNT (688.99±21.76 Wm^{-1}K^{-1}). Furthermore, thermal conductivity of CNT@BNNT is lower than that of BNNT@CNT (457.84±22.35 Wm^{-1}K^{-1}), which is also between the values of corresponding SWBNNT (252.04±18.12 Wm^{-1}K^{-1}) and SWCNT (609.98±31.92 Wm^{-1}K^{-1}), due to the higher thermal conductivity of larger SWCNT.

Temperature can significantly affect thermal transport in materials by dominating phonon scattering. Here, temperature dependence of thermal conductivity is investigated. Thermal conductivity of CNT@BNNT is calculated in the temperature range from 300 K to 1100 K, where the length and the inner diameter are fixed at 10 nm and 1.5 nm, respectively. As shown in Fig. 2b, thermal conductivity decreases with the increase of temperature, and it drops more than 66% down to 125.12±9.42 Wm^{-1}K^{-1} when temperature reaches 1100 K. Generally, thermal conductivity decreases proportional to 1/T due to the enhancement of Umklapp three-phonon scattering process. However, thermal conductivity of such a short CNT@BNNT decreases a little slower than the trend that is proportional to 1/T. The reason for the slower decrease trend may be ascribed to the shortage of Umklapp phonon-phonon scattering process. Here, the short length of only 10 nm could trigger the phonon-boundary scattering, which can lead to the shortage of phonon-phonon scatterings. A similar temperature dependence is also found in the studies on thermal conductivity of SWCNT [30–35]. On the other hand, an experimental study on a much longer SWCNT with a length of 2.6 μm shows that thermal conductiv-
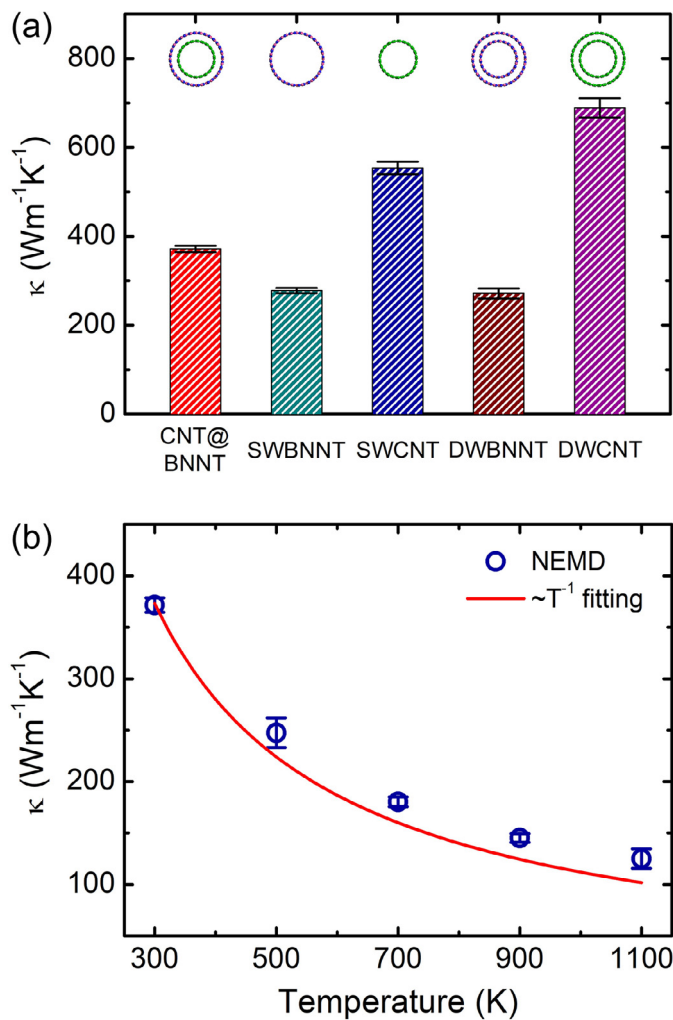
Fig. 2. (a) The comparison of thermal conductivity of CNT@BNNT and several nanotubes (SWBNNT, SWCNT, DWBNNT, DWCNT and BNNT@CNT) with the same length of 10 nm at room temperature; (b) Temperature dependence of thermal conductivity of CNT@BNNT. The length and the inner diameter are 10 nm and 1.5 nm, respectively.
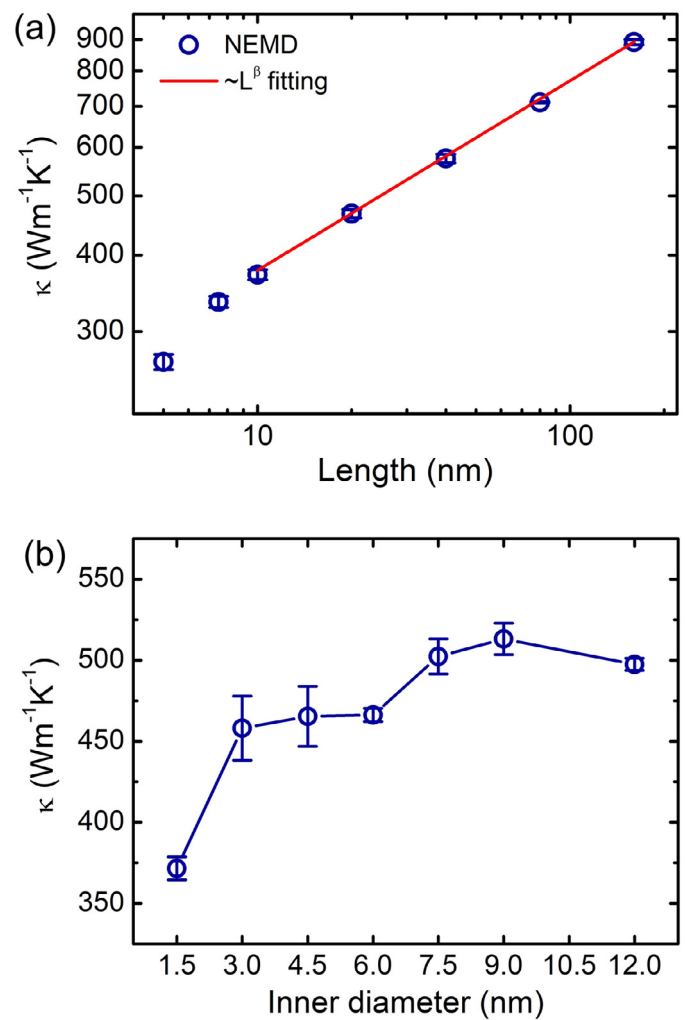

Fig. 3. Thermal conductivity of CNT@BNNT as a function of (a) length (the inner diameter is fixed at 1.5 nm) and (b) inner diameter (the length is fixed at 10 nm) at room temperature. The fitting value of β is 0.31±0.02.

ity can decrease a little steeper than 1/T, which could result from high-order phonon-phonon scatterings [36].

Size effect of thermal conductivity occurs when system size is reduced to nanoscale. So, it is necessary to study size dependence of thermal conductivity for CNT@BNNT. Firstly, length dependence of thermal conductivity is studied. Thermal conductivity is calculated in the length range from 5 nm to 160 nm at 300 K, where the inner diameter is fixed at 1.5 nm. As shown in Fig. 3a, thermal conductivity increases with the increase of length, it is obtained as high as 861.67±9.06 $Wm^{-1}K^{-1}$ when length reaches 160 nm. Noting that size confinement can arise in the nanoscale system, that is, phonon mean free path (MFP) is limited due to phonon-boundary scattering. Although thermal conductivity keeps increasing with length as the effective MFP of ballistic phonons increases, the gradient of profile gradually decreases since the number of ballistic phonons decreases. This suggests the increase of thermal conductivity is caused by the phonons with relatively long MFP compared to length. After the length of about 10 nm, thermal conductivity can be well fitted by an exponential function, which indicates that thermal conductivity increases proportional to L^{β} with a β value of 0.31±0.02. The anomalous length dependence of thermal conductivity as $\kappa \propto L^{\beta}$ (0<β≤1) has been reported in most of one-dimensional structures [33,34,37–42].

Secondly, diameter dependence of thermal conductivity is studied. The overall diameter is changed by adjusting the inner and outer diameter simultaneously, where the distance between inner and outer wall is maintained at an equilibrium interlayer distance, 0.34 nm. Thermal conductivity of CNT@BNNT is calculated at different inner diameters at 300 K, where the length is fixed at 10 nm. As shown in Fig. 3b, thermal conductivity increases with the increase of inner diameter. Such a diameter dependence of thermal conductivity was also reported in previous study on other nanotubes [43]. There are two aspects mainly account for the increasing thermal conductivity: 1) the number of phonon mode increases with the increase of inner diameter so that more phonons could participate in thermal transport; 2) the increase of inner diameter also leads to the reduction of curvature, which decreases the phonon scattering induced by curve strain. Eventually, thermal conductivity reaches a convergent value around 500 $Wm^{-1}K^{-1}$ when inner diameter is larger than 7.5nm, which is due to the saturation of phonon scattering.

Modulating thermal conductivity is important for thermal management in practical application, as well as understanding the mechanism that governs thermal transport [44–49]. Strain often occurs in a heterostructure as different atomic layers could have distinct coefficients of thermal expansion [50]. This is particularly true in the 1D case as the material is synthesized at high tem-
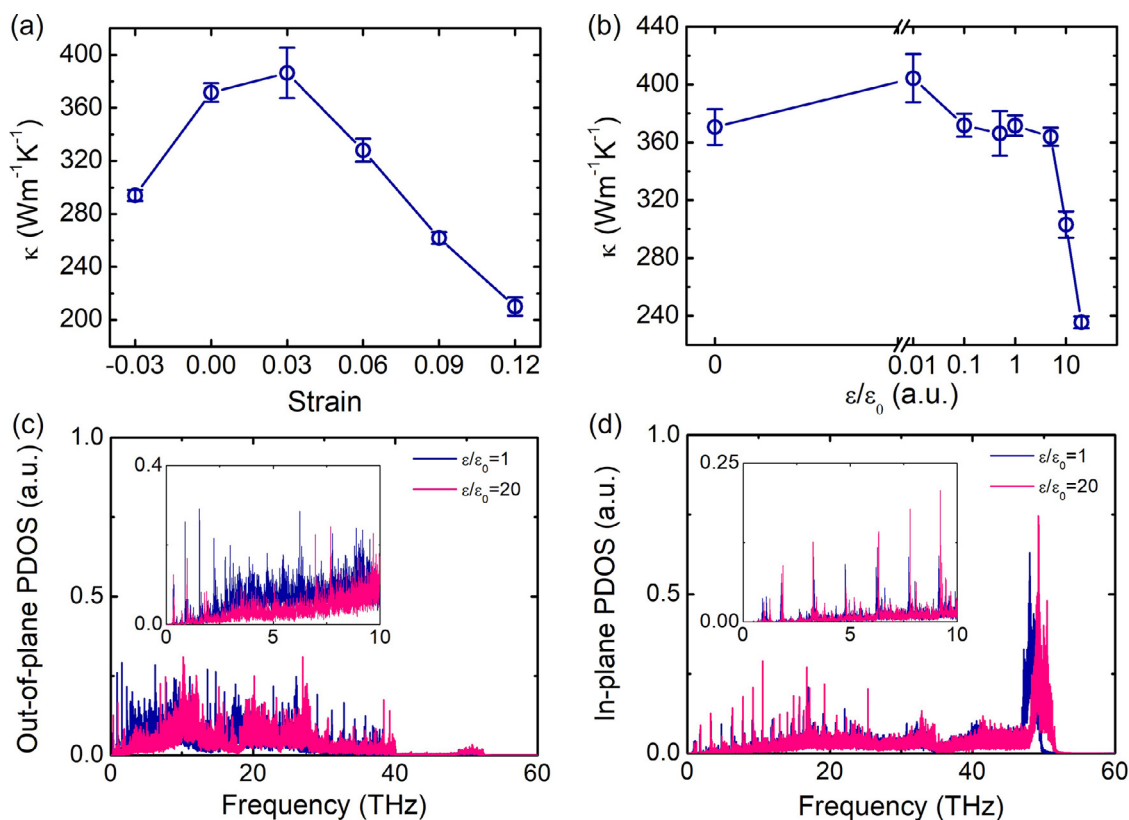
Fig. 4. Thermal conductivity of CNT@BNNT as a function of (a) strain along axial direction and (b) normalized intensity of vdW interaction between inner and outer nanotube. The length and the inner diameter are fixed at 10 nm and 1.5 nm respectively; (c) Out-of-plane (radial direction) and (d) in-plane (axial direction) phonon density of states for different intensities of vdW interaction, the insects show the low-frequency region of spectra.

peratures and, like 2D heterostructures, strain in a nested nanotube cannot be easily released due to it seamless geometry. Naturally, the mechanical strain is introduced to modulate thermal conductivity of CNT@BNNT. Note that the mechanical strain is applied along axial direction of heterostructure. Thermal conductivity of CNT@BNNT with different strain ranges from −0.03 to 0.12 is calculated at 300 K, where the length and the inner diameter are fixed at 10 nm and 1.5 nm, respectively. As shown in **Fig. 4a**, thermal conductivity has a strong dependence on strain, it decreases when heterostructure undergoes compression or stretch. When strain decreases to −0.03 under compression, thermal conductivity decreases to 294 ± 4.17 $Wm^{-1}K^{-1}$, which is reduced about 21% compared with the value of primitive heterostructure. Thermal conductivity decreases almost linearly with the increase of strain larger than 0.03, and it is reduced about 43% to 210.15 ± 6.88 $Wm^{-1}K^{-1}$ when strain reaches 0.12 under stretch. Previous studies have demonstrated that the strain effect of thermal conductivity is ascribed to the reduction of phonon group velocity, as well as the reduction of phonon relaxation time induced by the increase of the phase space of phonon scattering [34]. This result demonstrates that introducing mechanical strain is an efficient strategy to modulate thermal conductivity of CNT@BNNT.

Van der Waals interaction plays an important role between the inner and outer nanotube in heterostructures. Recognizing this, tuning intensity of interaction between two coaxial nanotubes is proposed to modulate thermal conductivity of CNT@BNNT. The intensity of interaction is adjusted by artificially changing the well depth in Lennard-Jones potential. Here the unitless parameter $\varepsilon/\varepsilon_0$ is defined as the ratio between artificial and original well depth, hence a larger value means more intense interaction and 0 indicates no interaction between inner and outer nanotube. Thermal conductivity of CNT@BNNT is calculated in the ratio range

from 0 to 20 at 300 K, where the length and the inner diameter are fixed at 10 nm and 1.5 nm, respectively. As shown in **Fig. 4b**, thermal conductivity has a strong dependence on intensity of interaction. With the ratio increases from 0 to 0.01, thermal conductivity slightly increases, indicating that a weaker interlayer interaction can slightly facilitate thermal transport. The reason for this facilitation is concluded to that the structural oscillation in out-of-plane that hinder in-plane thermal transport is depressed by the properly slight interaction. Then, thermal conductivity continues to decrease as the ratio increases, especially when the ratio is larger than 5, it has a rapid reduction. When the ratio reaches 20, thermal conductivity decreases 37% and a value of 235.55 ± 4.07 $Wm^{-1}K^{-1}$ is obtained. Previous studies have demonstrated that out-of-plane phonons dominate to impede the thermal transport in low-dimensional system. To explain the reduction of thermal conductivity, phonon density of states (PDOS) is calculated for both out-of-plane (radial) and in-plane (axial) direction. The PDOS spectra are obtained through performing Fourier transform on atomic velocity [15,34,35]. (Details are given in **supplementary material**) As shown in **Fig. 4c**, the number of low-frequency range out-of-plane phonons, which contribute more to thermal transport, decreases obviously when the intensity ratio increases from 1 to 20. However, there is no obvious difference in the in-plane PDOS in low-frequency range (shown in **Fig. 4d**). The reduction of thermal conductivity can be attributed to the depression of low-frequency out-of-plane phonons induced by intense interaction between CNT and BNNT. The result indicates that thermal conductivity of CNT@BNNT can be efficiently modulated by tuning intensity of the interaction between two coaxial nanotubes.

Different chiral single-wall nanotubes are formed through rolling up two-dimensional counterparts along different directions, and the structural diversity of CNT@BNNT can be gener-
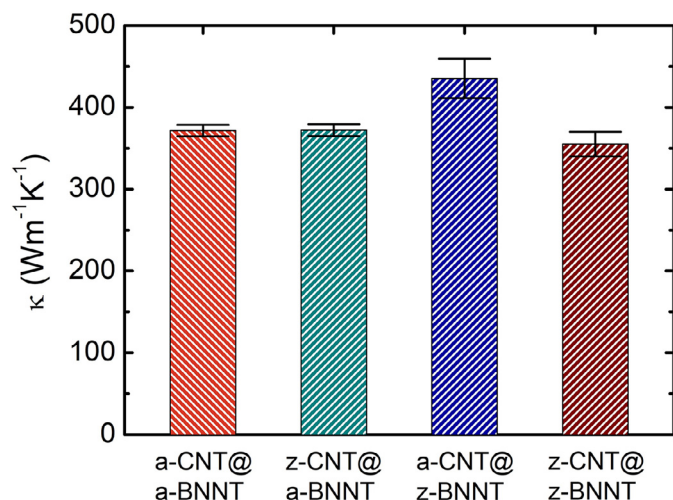
Fig. 5. Thermal conductivity of several structures of CNT@BNNT consist of different chiral CNT and BNNT at room temperature. The length and the inner diameter are fixed at 10 nm and 1.5 nm, respectively.

ated through alternating the chirality of constituent nanotubes. However, the chirality dependence of thermal conductivity remains blank and needs to be investigated. Due to the great amount of chirality, it is difficult and impossible to investigate all combinations. Therefore, we only focus on armchair and zigzag constituent CNT and BNNT (a-CNT, z-CNT and a-BNNT, z-BNNT) without considering other chirality. As shown in Fig. 5, thermal conductivity of CNT@BNNT with different chirality combination is calculated at 300 K, where the length and the inner diameter are fixed at 10 nm and 1.5 nm, respectively. The result shows that thermal conductivity of a-CNT@a-BNNT (371.61 ± 7.03 $Wm^{-1}K^{-1}$) and z-CNT@a-BNNT (372.18 ± 7.31 $Wm^{-1}K^{-1}$) are approximately the same. Among these four structures, a-CNT@z-BNNT and z-CNT@z-BNNT are calculated to have the highest and lowest thermal conductivity of 435.21 ± 24.20 $Wm^{-1}K^{-1}$ and 355.09 ± 15.02 $Wm^{-1}K^{-1}$, respectively. The result indicates that variation of the chirality of constituent nanotubes can make difference in thermal conductivity. However, the diversity of chirality is considered finitely so that the variation in combination of chiral nanotube is insufficient. More structures with different combination of chiral nanotubes need to be systematically studied in the future, and the highest and lowest thermal conductivity can be discovered by machine learning methodology, such as material informatics [51,52]. The reason for the structures with highest and lowest thermal conductivity needs to be revealed as well.

4. Conclusion

In this work, thermal conductivity of 1D heterostructure CNT@BNNT is systematically investigated by NEMD simulations. The result shows that thermal conductivity decreases proportional to the inverse of temperature from 300 to 1100 K, which indicates the dominant three-phonon scattering mechanism. Thermal conductivity increases proportional to the power function of length from 10 to 160 nm, and it also has a strong dependence on inner diameter in the range from 1.5 to 12 nm. The axial strain and intensity of interaction between inner and outer nanotubes are demonstrated to be able to modulate thermal conductivity. The dramatical reduction of thermal conductivity by axial strain is attributed to the decrease of phonon group velocity, as well as reduction of phonon relaxation time induced by the increase of the phase space of phonon scattering. The decrease of thermal conductivity induced by tuning intensity of interaction is ascribed to

the depression of low-frequency out-of-plane phonons. Moreover, the dependence of thermal conductivity on chirality of constituent nanotubes is also studied in the preliminary stage.

All in all, this work provides feasible strategies to modulate thermal conductivity of CNT@BNNT through temperature, size, strain and vdW interaction, which can be used for thermal management. The useful insights into the fundamental mechanisms that govern the thermal conductivity could be generalized to other 1D heterostructures and further facilitate their practical applications in optical and electronic devices.

Author statement

Han Meng: Investigation, Methodology, Software, Calculation, Formal analysis, Writing-Original Draft. **Shigeo Maruyama, Rong Xiang and Nuo Yang:** Conceptualization, Formal analysis, Writing - Review & Editing, Supervision, Funding acquisition.

Declaration of Competing Interest

The authors declare that they have no known competing financial interests or personal relationships that could have appeared to influence the work reported in this paper.

Supplementary materials

Supplementary material associated with this article can be found, in the online version, at doi:10.1016/j.ijheatmasstransfer.2021.121773.

References

[1] J. Wu, Y. Liu, Y. Liu, Y. Cai, Y. Zhao, H.K. Ng, K. Watanabe, T. Taniguchi, G. Zhang, C.-W. Qiu, D. Chi, A.H.C. Neto, J.T.L. Thong, K.P. Loh, K. Hippalgaonkar, Large enhancement of thermoelectric performance in MoS2/h-BN heterostructure due to vacancy-induced band hybridization, Proc. Natl. Acad. Sci. 117 (25) (2020) 13929.

[2] S. Lukman, L. Ding, L. Xu, Y. Tao, A.C. Riis-Jensen, G. Zhang, Q.Y.S. Wu, M. Yang, S. Luo, C. Hsu, L. Yao, G. Liang, H. Lin, Y.-W. Zhang, K.S. Thygesen, Q.J. Wang, Y. Feng, J. Teng, High oscillator strength interlayer excitons in two-dimensional heterostructures for mid-infrared photodetection, Nat. Nanotechnol. 15 (8) (2020) 675–682.

[3] Y. Cai, G. Zhang, Y.-W. Zhang, Electronic properties of phosphorene/graphene and phosphorene/hexagonal boron nitride heterostructures, J. Phys. Chem. C 119 (24) (2015) 13929–13936.

[4] H. Meng, M. An, T. Luo, N. Yang, 2 - Thermoelectric applications of chalcogenides, in: X. Liu, S. Lee, J.K. Furdyna, T. Luo, Y.-H. Zhang (Eds.), Chalcogenide, Woodhead Publishing, 2020, pp. 31–56.

[5] R. Xiang, T. Inoue, Y. Zheng, A. Kumamoto, Y. Qian, Y. Sato, M. Liu, D. Tang, D. Gokhale, J. Guo, K. Hisama, S. Yotsumoto, T. Ogamoto, H. Arai, Y. Kobayashi, H. Zhang, B. Hou, A. Anisimov, M. Maruyama, Y. Miyata, S. Okada, S. Chiashi, Y. Li, J. Kong, E.I. Kauppinen, Y. Ikuhara, K. Suenaga, S. Maruyama, One-dimensional van der Waals heterostructures, Science 367 (6477) (2020) 537–542.

[6] R. Xiang, S. Maruyama, Heteronanotubes: challenges and opportunities, Small Science (2021) 2000039.

[7] S. Cambre, M. Liu, D. Levshov, K. Otsuka, S. Maruyama, R. Xiang, Nanotube-based one-dimensional heterostructures coupled by van der Waals forces, arXiv:2107.09910.

[8] M.G. Burdanova, R.J. Kashtiban, Y. Zheng, R. Xiang, S. Chiashi, J.M. Woolley, M. Staniforth, E. Sakamoto-Rablah, X. Xie, M. Broome, J. Sloan, A. Anisimov, E.I. Kauppinen, S. Maruyama, J. Lloyd-Hughes, Ultrafast optoelectronic processes in 1D radial van der Waals heterostructures: carbon, boron nitride, and MoS_2 nanotubes with coexisting excitons and highly mobile charges, Nano Lett. 20 (5) (2020) 3560–3567.

[9] Y. Qian, S. Seo, I. Jeon, H. Lin, S. Okawa, Y. Zheng, A. Shawky, A. Anisimov, E.I. Kauppinen, J. Kong, R. Xiang, Y. Matsuo, S. Maruyama, MoS_2-carbon nanotube heterostructure as efficient hole transporters and conductors in perovskite solar cells, Appl. Phys. Express 13 (7) (2020) 075009.

[10] X. Liu, J. Gao, G. Zhang, Y.-W. Zhang, Design of phosphorene/graphene heterojunctions for high and tunable interfacial thermal conductance, Nanoscale 10 (42) (2018) 19854–19862.

[11] K. Ren, X. Liu, S. Chen, Y. Cheng, W. Tang, G. Zhang, Remarkable reduction of interfacial thermal resistance in nanophononic heterostructures, Adv. Funct. Mater. 30 (42) (2020) 2004003.

[12] Y. Cai, Q.-X. Pei, G. Zhang, Y.-W. Zhang, Decoupled electron and phonon transports in hexagonal boron nitride-silicene bilayer heterostructure, J. Appl. Phys. 119 (6) (2016) 065102.

[13] N. Mingo, L. Yang, J. Han, M.P. Anantram, Resonant versus anti-resonant tunneling at carbon nanotube A–B–A heterostructures, Phys. Status Solidi 226 (1) (2001) 79–85.

[14] M. An, H. Meng, T. Luo, N. Yang, 11 - Thermal transport of chalcogenides, in: X. Liu, S. Lee, J.K. Furdyna, T. Luo, Y.-H. Zhang (Eds.), Chalcogenide, Woodhead Publishing, 2020, pp. 339–370.

[15] M. An, Q. Song, X. Yu, H. Meng, D. Ma, R. Li, Z. Jin, B. Huang, N. Yang, Generalized two-temperature model for coupled phonons in nanosized graphene, Nano Lett. 17 (9) (2017) 5805–5810.

[16] D. Ma, X. Wan, N. Yang, Unexpected thermal conductivity enhancement in pillared graphene nanoribbon with isotopic resonance, Phys. Rev. B 98 (24) (2018) 245420.

[17] D. Ma, A. Arora, S. Deng, G. Xie, J. Shiomi, N. Yang, Quantifying phonon particle and wave transport in silicon nanophononic metamaterial with cross junction, Mater. Today Phys. 8 (2019) 56–61.

[18] M. An, L. Li, S. Hu, Z. Ding, X. Yu, B. Demir, N. Yang, W. Ma, X. Zhang, Mass difference and polarization lead to low thermal conductivity of graphene-like carbon nitride (C3N), Carbon 162 (2020) 202–208.

[19] X. Wei, T. Luo, Chain length effect on thermal transport in amorphous polymers and a structure–thermal conductivity relation, PCCP 21 (28) (2019) 15523–15530.

[20] X. Wan, D. Ma, D. Pan, L. Yang, N. Yang, Optimizing thermal transport in graphene nanoribbon based on phonon resonance hybridization, Mater. Today Phys. 20 (2021) 100445.

[21] S. Plimpton, Fast parallel algorithms for short-range molecular dynamics, J. Comput. Phys. 117 (1) (1995) 1–19.

[22] M. An, B. Demir, X. Wan, H. Meng, N. Yang, T.R. Walsh, Predictions of thermo-mechanical properties of cross-linked polyacrylamide hydrogels using molecular simulations, Adv. Theory Simul. 2 (3) (2019) 1800153.

[23] D. Ma, H. Ding, H. Meng, L. Feng, Y. Wu, J. Shiomi, N. Yang, Nano-cross-junction effect on phonon transport in silicon nanowire cages, Phys. Rev. B 94 (16) (2016) 165434.

[24] X. Yu, R. Li, T. Shiga, L. Feng, M. An, L. Zhang, J. Shiomi, N. Yang, Hybrid thermal transport characteristics of doped organic semiconductor poly(3,4-ethylenedioxythiophene):tosylate, J. Phys. Chem. C 123 (43) (2019) 26735–26741.

[25] X.-Y. Mi, X. Yu, K.-L. Yao, X. Huang, N. Yang, J.-T. Lü, Enhancing the thermoelectric figure of merit by low-dimensional electrical transport in phonon-glass crystals, Nano Lett. 15 (8) (2015) 5229–5234.

[26] L. Lindsay, D.A. Broido, Optimized Tersoff and Brenner empirical potential parameters for lattice dynamics and phonon thermal transport in carbon nanotubes and graphene, Phys. Rev. B 81 (20) (2010).

[27] C. Sevik, A. Kinaci, J.B. Haskins, T. Çağın, Characterization of thermal transport in low-dimensional boron nitride nanostructures, Phys. Rev. B 84 (8) (2011) 085409.

[28] A.K. Rappe, C.J. Casewit, K.S. Colwell, W.A. Goddard, W.M. Skiff, UFF, a full periodic table force field for molecular mechanics and molecular dynamics simulations, J. Am. Chem. Soc. 114 (25) (1992) 10024–10035.

[29] W.C. Swope, H.C. Andersen, P.H. Berens, K.R. Wilson, A computer simulation method for the calculation of equilibrium constants for the formation of physical clusters of molecules: application to small water clusters, J. Chem. Phys. 76 (1) (1982) 637–649.

[30] A. Javey, J. Guo, M. Paulsson, Q. Wang, D. Mann, M. Lundstrom, H. Dai, High–field quasiballistic transport in short carbon nanotubes, Phys. Rev. Lett. 92 (10) (2004) 106804.

[31] M. Grujicic, G. Cao, W.N. Roy, Computational analysis of the lattice contribution to thermal conductivity of single-walled carbon nanotubes, J. Mater. Sci. 40 (8) (2005) 1943–1952.

[32] J. Che, T. Çağın, W. Deng, W.A.G. III, Thermal conductivity of diamond and related materials from molecular dynamics simulations, J. Chem. Phys. 113 (16) (2000) 6888–6900.

[33] S. Maruyama, A molecular dynamics simulation of heat conduction of a finite length single-walled carbon nanotube, Microscale Thermophys. Eng. 7 (1) (2003) 41–50.

[34] H. Meng, D. Ma, X. Yu, L. Zhang, Z. Sun, N. Yang, Thermal conductivity of molybdenum disulfide nanotube from molecular dynamics simulations, Int. J. Heat Mass Transfer 145 (2019) 118719.

[35] H. Meng, X. Yu, H. Feng, Z. Xue, N. Yang, Superior thermal conductivity of poly (ethylene oxide) for solid-state electrolytes: a molecular dynamics study, Int. J. Heat Mass Transfer 137 (2019) 1241–1246.

[36] E. Pop, D. Mann, Q. Wang, K. Goodson, H. Dai, Thermal conductance of an individual single-wall carbon nanotube above room temperature, Nano Lett. 6 (1) (2006) 96–100.

[37] S. Maruyama, A molecular dynamics simulation of heat conduction in finite length SWNTs, Physica B 323 (1) (2002) 193–195.

[38] N. Mingo, D.A. Broido, Length dependence of carbon nanotube thermal conductivity and the "problem of long waves, Nano Lett. 5 (7) (2005) 1221–1225.

[39] G. Zhang, B. Li, Thermal conductivity of nanotubes revisited: effects of chirality, isotope impurity, tube length, and temperature, J. Chem. Phys. 123 (11) (2005) 114714.

[40] J. Shiomi, S. Maruyama, Molecular dynamics of diffusive-ballistic heat conduction in single-walled carbon nanotubes, Japan. J. Appl. Phys. 47 (4) (2008) 2005–2009.

[41] J. Shiomi, S. Maruyama, Diffusive-ballistic heat conduction of carbon nanotubes and nanographene ribbons, Int. J. Thermophys. 31 (10) (2010) 1945–1951.

[42] N. Yang, G. Zhang, B. Li, Violation of Fourier's law and anomalous heat diffusion in silicon nanowires, Nano Today 5 (2) (2010) 85–90.

[43] L. Lindsay, D.A. Broido, N. Mingo, Diameter dependence of carbon nanotube thermal conductivity and extension to the graphene limit, Phys. Rev. B 82 (16) (2010) 161402.

[44] M. Dengke, L. Xiuling, Z. Lifa, Tuning thermal transport via phonon localization in nanostructures, Chin. Phys. B (2020).

[45] C. Shao, X. Yu, N. Yang, Y. Yue, H. Bao, A review of thermal transport in low-dimensional materials under external perturbation: effect of strain, substrate, and clustering, Nanoscale Microscale Thermophys. Eng. 21 (4) (2017) 201–236.

[46] E. Lee, T. Luo, Thermal transport across solid-solid interfaces enhanced by pre-interface isotope-phonon scattering, Appl. Phys. Lett. 112 (1) (2018) 011603.

[47] R. Shrestha, P. Li, B. Chatterjee, T. Zheng, X. Wu, Z. Liu, T. Luo, S. Choi, K. Hippalgaonkar, M.P. de Boer, S. Shen, Crystalline polymer nanofibers with ultra-high strength and thermal conductivity, Nat. Commun. 9 (1) (2018) 1664.

[48] Z. Zhang, S. Hu, T. Nakayama, J. Chen, B. Li, Reducing lattice thermal conductivity in schwarzites via engineering the hybridized phonon modes, Carbon 139 (2018) 289–298.

[49] X. Yu, D. Ma, C. Deng, X. Wan, M. An, H. Meng, X. Li, X. Huang, N. Yang, How does van der waals confinement enhance phonon transport? Chin. Phys. Lett. 38 (1) (2021) 014401.

[50] W. Pan, J. Xiao, J. Zhu, C. Yu, G. Zhang, Z. Ni, K. Watanabe, T. Taniguchi, Y. Shi, X. Wang, Biaxial compressive strain engineering in graphene/boron nitride heterostructures, Sci. Rep. 2 (1) (2012) 893.

[51] X. Wan, W. Feng, Y. Wang, H. Wang, X. Zhang, C. Deng, N. Yang, Materials discovery and properties prediction in thermal transport via materials informatics: a mini review, Nano Lett. 19 (6) (2019) 3387–3395.

[52] S. Ju, J. Shiomi, Materials informatics for heat transfer: recent progresses and perspectives, Nanoscale Microscale Thermophys. Eng. 23 (2) (2019) 157–172.

<u>**Supplementary material**</u>

Thermal conductivity of one-dimensional carbon-boron nitride van der Waals heterostructure: A molecular dynamics study

Han Meng[a, b], Shigeo Maruyama[b], Rong Xiang[b, *], Nuo Yang[a, *]

[a] State Key Laboratory of Coal Combustion, School of Energy and Power Engineering, Huazhong University of Science and Technology, Wuhan 430074, China.

[b] Department of Mechanical Engineering, The University of Tokyo, 7-3-1 Hongo, Bunkyo-ku, Tokyo 113-8656, Japan.

* Corresponding author.
E-mail address: xiangrong@photon.t.u-tokyo.ac.jp (R. X.) and nuo@hust.edu.cn (N. Y.)

S1. The molecular dynamics simulation details.

All NEMD simulation details are provided in table S1. The simulation procedure is summarized as follows. After minimization, a100 ps NPT ensemble is used to relax the structure. Then, a 100 ps NVE ensemble to reach the steady state for the system except the thermostat region. Finally, a 5 ns NVE ensemble is used to record and average the temperature and heat flux.

Table S1. Molecular dynamics simulation details

Method		Non-Equilibrium molecular dynamics	
Potential		Tersoff	
	Lennard-Jones	ε_{C-B}= 5.962×10^{-3} eV, σ_{C-B}=3.534 Å ε_{C-N}= 3.691×10^{-3} eV, σ_{C-N}=3.346 Å	
Time step	0.5 fs	**Thermostat**	Langevin
Simulation process			
Ensemble	**Setting**		**Purpose**
NPT	Boundary condition	x, y, z: p, p, p	Relax structure
	Runtime	100 ps	
NVE	Boundary condition	x, y, z: p, p, f	Reach steady state
	Runtime	100 ps	
NVE	Boundary condition	x, y, z: p, p, f	Record information
	Runtime	5 ns	
Recorded physical quantity			
Temperature		$\langle E \rangle = \sum_{i=1}^{N} \frac{1}{2} m_i v_i^2 = \frac{3}{2} N k_B T$	
Heat flux		$J = \dfrac{\Delta E_{in} + \Delta E_{out}}{2\Delta t}$	
Thermal conductivity		$\kappa = -\dfrac{J}{A\nabla T} = -\dfrac{JL}{A\Delta T}$	
Phonon density of states		$D(\omega) = \dfrac{\sum m |\int v(t) exp(-i\omega t) dt|^2}{N k_B T}$	

S2. Temperature and energy of molecular dynamics simulation.
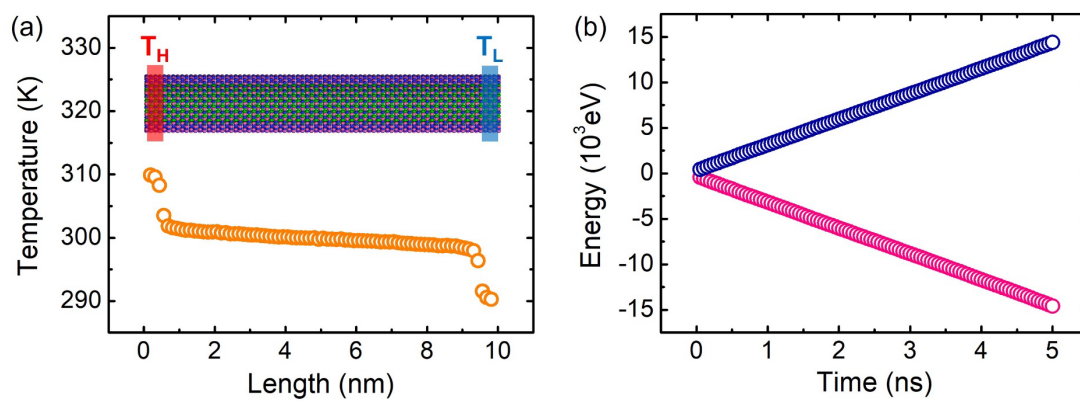

Fig. S1. (a) Schematic NEMD simulation setup and time-averaged temperature profile; (b) Accumulated energy change of heat bath and heat sink after the system reaches steady state.